

Short Communication

Study on the Corrosion Behaviours of X80 Pipeline Steel Joints Fabricated via Hot-Wire Tungsten Inert Gas Welding

Yao Zongxiang^{1,2}, Jiang Shan¹, Wang Gang^{1,*}, Yin limeng^{1,*}, Jiang Deping³, Zhang Zhongwen¹

¹ School of Metallurgy and Materials Engineering, Chongqing University of Science and Technology, Chongqing 401331, China

² Material Corrosion and Protection Key Laboratory of Sichuan Province, Zigong 643000, China

³ School of Electrical Engineering, Chongqing University of Science and Technology, Chongqing 401331, China

*Email: wwg_16@163.com, yeenlm@163.com

Received: 7 November 2018 / Accepted: 15 January 2019 / Published: 7 February 2019

X80 pipeline steel joints were fabricated via hot-wire tungsten inert gas welding by using ER70S-G wire with a diameter of 1.2 mm. The microstructures of the welded joints were analysed by using metallographic microscopy. Weight-loss methods, polarization curve measurements and electrochemical impedance spectroscopy (EIS) techniques were used to analyse the corrosion behaviours of the X80 pipeline steel welded joints in a 3.5% NaCl solution. The corrosion products and morphologies were characterized by X-ray diffraction (XRD) and scanning electron microscopy (SEM). The results show that the microstructure of the weld zone is composed of acicular ferrite, whereas the microstructure of the heat-affected zone is mainly composed of granular bainite, bainite ferrite, and a small amount of striated M-A. The corrosion weight-loss of the heat-affected zone is greater than those of the base metal and weld zone. Electrochemical testing results indicate that the corrosion current potential of the heat-affected zone is lower than those of the base metal and weld zone. Moreover, the corrosion current in the heat-affected zone is higher and its impedance is also lower than those of the base metal and weld zone. Furthermore, the heat-affected zone is more susceptible to corrosion than the base metal and weld zone. This susceptibility to corrosion is due to the electrochemical reaction that is driven by the potential difference between the coarse bainite ferrite and the non-equilibrium GB, which causes corrosion failure of the material in the corrosive medium.

Keywords: X80 pipeline steel; hot-wire tungsten inert gas welding; electrochemical properties; corrosion behaviour; polarization curve

1. INTRODUCTION

With the increasing demand for oil and natural gas resources, the strength demands of pipeline steel are also increasing. In recent decades, the strength of pipeline steel has varied from X70 to X80.

As the strength of the metal increases, the stress corrosion resistance of the metal will be reduced significantly[1-2]. High-grade X80 pipeline steel has been successfully used in building "West-East" gas pipelines [3-5]. The weldability and corrosion resistance of pipeline steel have attracted substantial attention during pipeline construction and service. Generally, pipelines buried in the ground are mainly corroded by water, oxygen and microorganisms in the soil; moreover, the PH of most soils is in the range of 6-7. Pipelines that are in contact with different types of soil may suffer from corrosion in their operation. Once corrosion occurs, it will cause huge economic losses and adverse consequences[6]. Therefore, pipeline safety is very important in oil and natural gas long-distance transmission systems.

It is extremely important to research the corrosion resistances of welded joints under complex conditions[7]. Currently, most studies on the corrosion of X80 pipeline steel have focused on its stress corrosion behaviour [6,8-13]. However, studies on the corrosion behaviour of hot-wire tungsten inert gas (TIG)-welded joints of X80 have rarely been reported[13]. Therefore, to ensure the safety and reliability of X80 pipeline steel, the corrosion properties of X80 welded joints should be investigated. Accordingly, welded joints composed of X80 steel were investigated in this study. The object of this paper was to study the corrosion properties of X80 welded joints in 3.5% NaCl solutions and analyse the different corrosion morphologies of the steel after polarization.

2. EXPERIMENTAL METHODS

X80 spiral-welded pipeline steel from China is used for the experiments, and Table 1 shows its chemical composition (wt.%). The X80 pipeline steel used for welding in the experiment was cut into 500 mm×150 mm×18.4 mm samples via wire-cutting. The welding method was hot-wire TIG welding, ER70S-G welding wire was adopted, and single-sided welding was processed. Fig. 1 shows the type of welding groove used in this study. The welding parameters are shown in Table 2. Before welding, the 30~50 mm widths on both sides of the groove were eliminated by using a grinding disc. After welding, the size of each metallographic sample acquired from the welding area was approximately 4 mm×10 mm×20 mm. The metallographic samples were corroded with 4% alcohol nitrate solutions after grinding and polishing. Then, the microstructures of different areas in the welded joints were observed with a Leica DM2500M series microscope.

Table 1. Chemical composition of the X80 pipeline steel (wt.%)

C	Mn	Cr	Si	Mo	Nb	Ti	V	Ni	Fe
0.0193	1.9400	0.2730	0.2040	0.0742	0.0622	0.0123	0.0036	0.2670	allowance

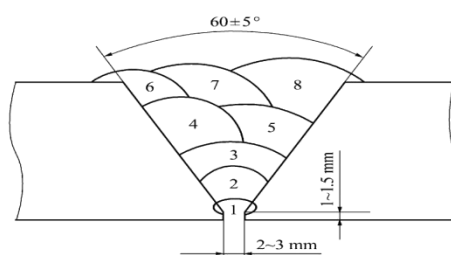


Figure 1. Welding groove type

Table 2. Hot-wire TIG welding parameters

Weld bead	Electric current (A)	Voltage (V)	Wire feed speed (cm·min ⁻¹)	Gas flow rate (L·min ⁻¹)	Wire diameter (mm)
Welding root	140	9~11	140	15	1.2
Fill layer	200	9~11	280	15	1.2
Cover layer	160	9~11	200	15	1.2

Two types of corrosion samples were cut from the welded joints via wire-cutting. Each sample had dimensions of 15 mm × 15 mm × 2 mm (the surface area was 570 mm²) for the immersion tests. In these experiments, the solution was 3.5% NaCl (pH of 6). This solution consisted of pure NaCl and distilled water. The soaking time was 20×24 h at room temperature (18±2°C). The sample size used for all electrochemical tests was 10 mm×10 mm×2 mm. Before each group of corrosion tests, the surfaces of all the samples were polished with sandpaper up to 1500#, and then the samples were rinsed with absolute ethanol via ultrasonication, washed with deionized water, dried and placed in a drying vessel. Scanning electron microscopy (SEM) and X-ray diffraction (XRD) were employed to analyse the corrosion morphologies and products. The corrosion product film on the surface of the sample was removed with a removal liquid (500 mL hydrochloric acid +500 mL deionized water + 315 g hexamethylenetetramine). After cleaning and drying, the corroded samples were weighed with a precision electronic balance, and the weights were recorded. The corrosion rates of the X80 steel base metal (BM), weld zone (WZ) and heat-affected zone (HAZ) were calculated by using formula 1. All weight-loss tests were carried out in parallel for the three groups in the solution to verify the repeatability.

$$V = (W_0 - W_t) / S t \quad (1)$$

In formula 1, V is the corrosion rate (g/(m²·h)); W₀ is the sample weight before corrosion (g); W_t is the weight after corrosion (g); S is the sample surface area (m²); and t is the etch time (h).

The open-circuit potential (OCP), polarization curves and electrochemical impedance spectroscopy (EIS) results were measured by PARSTAT 4000A (Princeton, USA) electrochemical workstation. Three electrode systems with volumes of 0.5 L were used in all electrochemical experiments. The area of the test sample exposed to the 3.5% NaCl solution was 1 cm². The three electrodes were the working electrode, a platinum sheet (20 mm × 10 mm) used as the auxiliary electrode, and a saturated calomel electrode (SCE) that acted as the reference electrode. In the experiment, when the samples of the X80 welded joints were immersed in the 3.5% solution for 0.5 h, the stable potential was determined via the OCP measurement method. During the potential dynamic polarization curve test, the scanning speed was 0.5 mV/s, and the scanning potential was -0.8~1.0 V. The EIS results were measured at the open-circuit potential. The frequency range of the impedance spectroscopy was 100 kHz to 100 MHz, and the amplitude of the AC signal voltage was 5 mV. The polarization curves were fitted by Origin8.0. ZSimpWin was used to analyse AC impedance data.

3. RESULTS AND DISCUSSION

3.1 Microstructures of the X80 welded joints

Fig. 2 shows the microstructures of the different zones of the X80 joint fabricated via hot-wire TIG welding. It can be found from Fig. 2 that the microstructure of BM is a mixed structure that mainly consists of granular bainite (GB) and a small amount of polygonal ferrite (PF), as shown in Fig. 2(a). Moreover, the BM exhibited a fine and uniform structure. The microstructure of the MZ mainly consists of acicular ferrite (AF), which is intersected with a woven basket, and no obvious coarse Widmanstätten structures were observed, as shown in Fig. 2(b). The microstructure of the HAZ was characterized by unevenly distributed coarse grains and a low dislocation density, and it is also a mixed structure that mainly consists of GB and bainite ferrite (BF) and a small amount of striated martensite-austenite (M-A) microstructures, as shown in Fig. 2(c). As a result of the thermal cycling from welding, the transformation of ferrite (α) into austenite (γ) can prevent high melting point carbon nitride (M(CN)) particles from dissolving and precipitating at higher temperatures, and the transformation promotes the growth of the austenite grains [15]. Moreover, because of the aggregation of carbon atoms, M-A constituents are formed on grain boundaries, which reduces the toughness values of the welded joints.

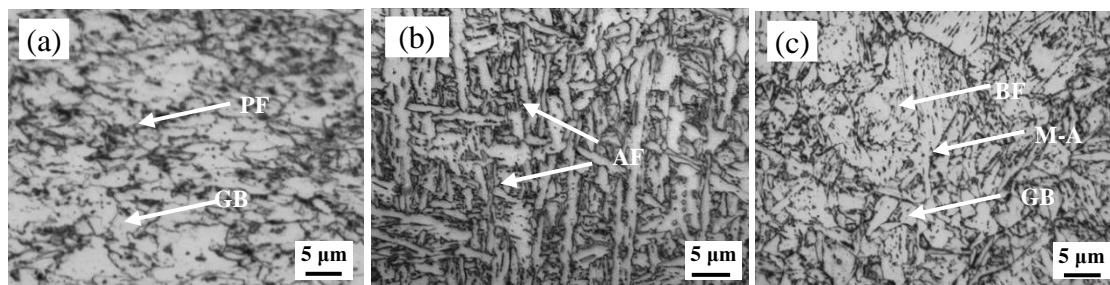


Figure 2. Microstructures of the hot-wire TIG-welded joints composed of X80 pipeline steel: (a) BM; (b) MZ; and (c) HAZ

3.2 Corrosion test results

3.2.1 Corrosion rates and corrosion morphologies

Table 3. Corrosion rates of the X80 steel welded joints after immersion in 3.5% NaCl solutions

Sample	Weight before corrosion, W_0 (g)	Weight after corrosion, W_t (g)	Weight loss, ΔW (g)	Corrosion rate, V ($\text{g}\cdot\text{m}^{-2}\cdot\text{h}^{-1}$)
BM	4.1809	4.1687	0.0122	0.04459
WZ	4.1820	4.1678	0.0142	0.05190
HAZ	4.1883	4.1738	0.0145	0.05300

Table 3 shows the results of the immersion tests. The weight losses and corrosion rates of the BM, WZ, and HAZ were 0.0122 g and $0.04459 \text{ g}\cdot\text{m}^{-2}\cdot\text{h}^{-1}$, 0.0142 g and $0.05190 \text{ g}\cdot\text{m}^{-2}\cdot\text{h}^{-1}$, and 0.0145 g

and $0.05300 \text{ g}\cdot\text{m}^{-2}\cdot\text{h}^{-1}$, respectively. The corrosion resistance of the BM is higher than those of the WZ and HAZ. The microstructure and composition inhomogeneity, the weld defects and stress concentrations reduce the corrosion resistance of the WZ. Because of the presence of coarse grains, the corrosion resistance of the HAZ, which is the weakest part of the welded joint, is low.

The surface morphologies of the different zones of the X80 welded joint after immersion in 3.5% NaCl solutions are shown in Fig. 3. Fig. 3 shows that the corrosion products of the BM after immersion in the 3.5% NaCl solution are distributed uniformly in a granular form, as shown in Fig. 3(a), which results in a good corrosion resistance. Fig. 3(b) shows the corrosion morphology of the WZ, wherein the corrosion products are unevenly distributed as laminae on the substrate. As shown in Fig. 3(c), the corrosion products in the HAZ had a wadding shape, and they were small, loose, and contained many gaps and holes, which results in the worst corrosion resistance among the tested zones of the samples. The corrosion product films on the surfaces of the MZ and HAZ have poor protection, which results in caustic ions, such as chloride ions, reacting with the matrix to cause corrosion. Therefore, the corrosion resistances of the WZ and HAZ are worse than that of the BM.

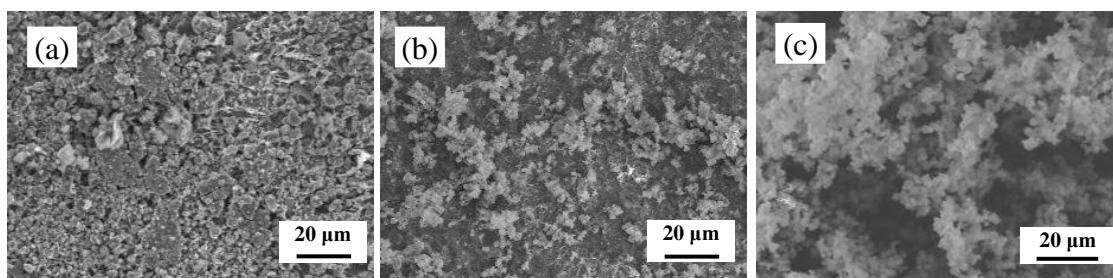


Figure 3. Corrosion morphologies of the different zones on the X80 welded joint after immersion in the 3.5% NaCl solution: (a) BM; (b) WZ; and (c) HAZ

Fig. 4 shows the surface morphologies of the different zones on the X80 welded joint after the removal of the corrosion products in a 3.5% NaCl solution for 20 days. The corrosion on the surface of the BM is relatively uniform, the local corrosion area is small, the number of pits is small, and the pittings are shallow. A small amount of pitting marks and microcracks are observed on the surface of the WZ. The HAZ has a greater number of pittings than WZ, and it has obvious cracks. Therefore, the extent of corrosion in the HAZ is significantly higher than that in the BM and WZ.

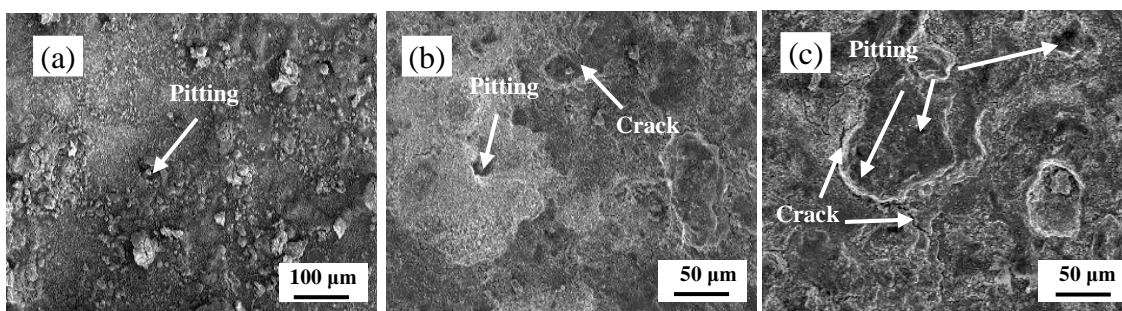


Figure 4. Surface morphologies of the X80 welded joints after removing the corrosion products: (a) BM; (b) WZ; and (c) HAZ

3.2.2 Polarization curves

The polarization behaviours of the different zones of the X80 welded joints after immersion in the 3.5% NaCl solution for 0.5 h are shown in Fig. 5. Fig. 5 shows that the shapes of the polarization curves in the three samples were similar. The obtained fitting parameters obtained by using the Tafel linear extrapolation method are revealed in Table 4. Table 4 shows that the corrosion current densities (i_{corr}) of the BM, WZ, and HAZ are $32.54 \mu\text{A}/\text{cm}^2$, $35.29 \mu\text{A}/\text{cm}^2$, and $42.07 \mu\text{A}/\text{cm}^2$, respectively. Therefore, the corrosion resistance of the HAZ is obviously inferior to those of the BM and WZ. The corrosion current potential (ΔE) can also often be seen as a measure of corrosion: the more the negative value of ΔE is, the greater the ability to lose electrons. Therefore, the sample corroded more easily when the corrosion current potential is more negative. The ΔE values of BM, WZ and HAZ are -711 mv, -728 mv, and -758 mv, respectively. The corrosion rates (V_1) of the BM, WZ, and HAZ are 0.3807 mm/a, 0.4129 mm/a and 0.4922 mm/a, respectively. Therefore, the electrocorrosion tendency of the HAZ is the greatest among the three zones.

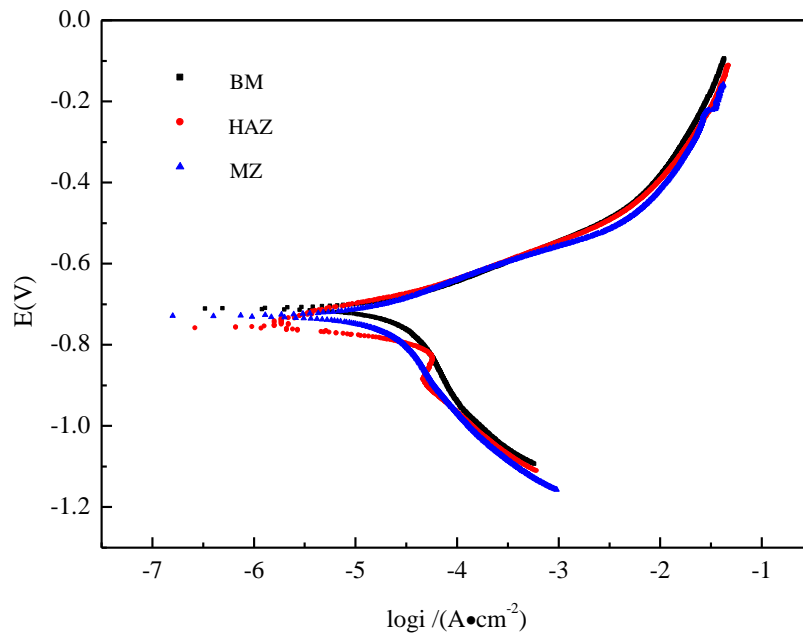


Figure 5. Polarization curves of the hot-wire TIG-welded joints composed of X80 pipeline steel in the 3.5% NaCl solution

Table 4. Results of the polarization curve fitting

Test sample	Corrosion potential, ΔE (mv)	Corrosion current density, i_{corr} ($\mu\text{A}\cdot\text{cm}^{-2}$)	Corrosion rate, V_1 ($\text{mm}\cdot\text{a}^{-1}$)
BM	-711	32.54	0.3807
WZ	-728	35.29	0.4129
HAZ	-758	42.07	0.4922

3.2.3 Impedance measurements

The electrochemical behaviours of the different zones of the X80 welded joint in the 3.5% NaCl solution are studied by using EIS. The Nyquist plots of the different parts are shown in Fig. 6. The variations in the Nyquist plot of the three parts exhibit similar characteristics. The impedance spectra were fitted with ZSimpWin software. The equivalent electrical circuit model, which is the best fit between the experimental data and the fitting results, is shown in Fig. 7. In Fig. 7, R_s is the solution resistance, R_{ct} is the charge transfer resistance, R_f is the resistance of the corrosion product on the electrode surface, C_f is the corrosion product capacitance, C_d is the electrical double-layer capacitance, C_m is the surface film capacitance, and R_m is the surface film resistance. In the equivalent circuit, the parameters of each component are shown in Table 5.

In general, the higher the value of R_{ct} is, the more difficult the electrode reaction. The smaller the corrosion rate is, the better the corrosion resistance of the material[16-17]. The charge transfer resistances of the BM, WZ and HAZ were $194.2 \Omega \cdot \text{cm}^2$, $188.1 \Omega \cdot \text{cm}^2$ and $147.9 \Omega \cdot \text{cm}^2$, respectively, in the 3.5% NaCl solution. The charge transfer resistance of the HAZ is obviously smaller than those of the BM and WZ, which indicates that the HAZ has poor corrosion resistance because of its low charge reaction resistance in the 3.5% NaCl solution.

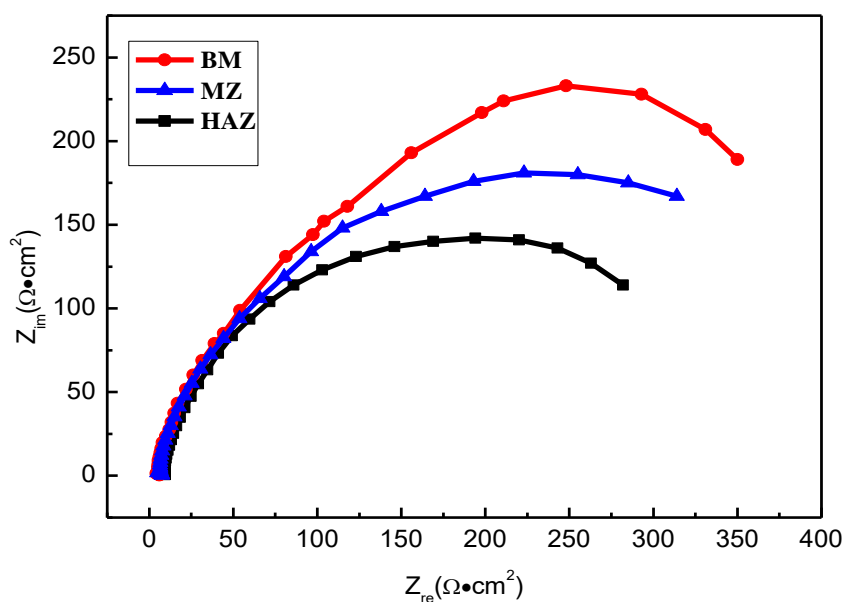


Figure 6. Nyquist plots of the different parts of the welded joint in the 3.5% NaCl solution

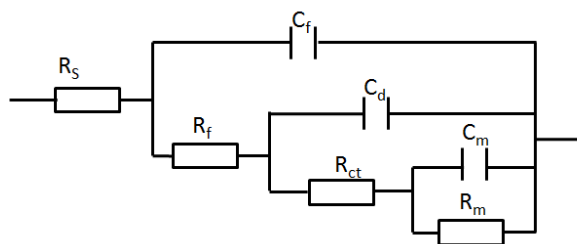


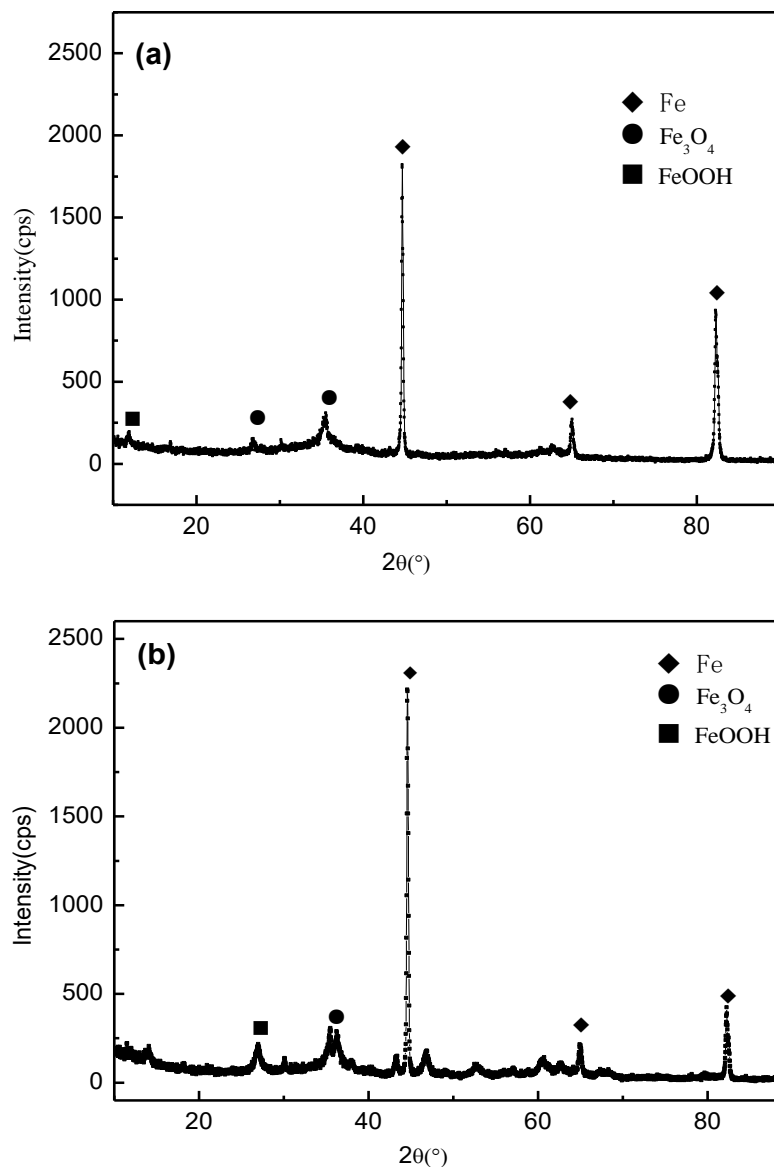
Figure 7. Equivalent electrical circuit model of the X80 welded joint in the 3.5% NaCl solution

Table 5. Electrochemical impedance fitting parameters from Fig. 7

Test sample	R_s ($\Omega \cdot \text{cm}^2$)	R_f ($\Omega \cdot \text{cm}^2$)	R_{ct} ($\Omega \cdot \text{cm}^2$)	C_f ($\text{F} \cdot \text{cm}^2$)	C_d ($\text{F} \cdot \text{cm}^2$)	C_m ($\text{F} \cdot \text{cm}^2$)	R_m ($\Omega \cdot \text{cm}^2$)
BM	38.57	60.98	186.7	4.131E-7	1.274E-4	2.196E-4	39.76
WZ	24.96	56.84	177.1	5.584 E-7	8.913E-3	5.524E-4	37.63
HAZ	3.28	28.51	142.3	3.517 E-6	2.347E-3	3.618E-3	17.21

3.2.4 Corrosion products analysis

X-ray diffraction was used to confirm the corrosion products on the surfaces of the samples; the results are shown in Fig. 8. The observed peaks closely correspond to Fe_3O_4 and FeOOH . During the formation of the corrosion products, the possible reactions are as follows[18-21].



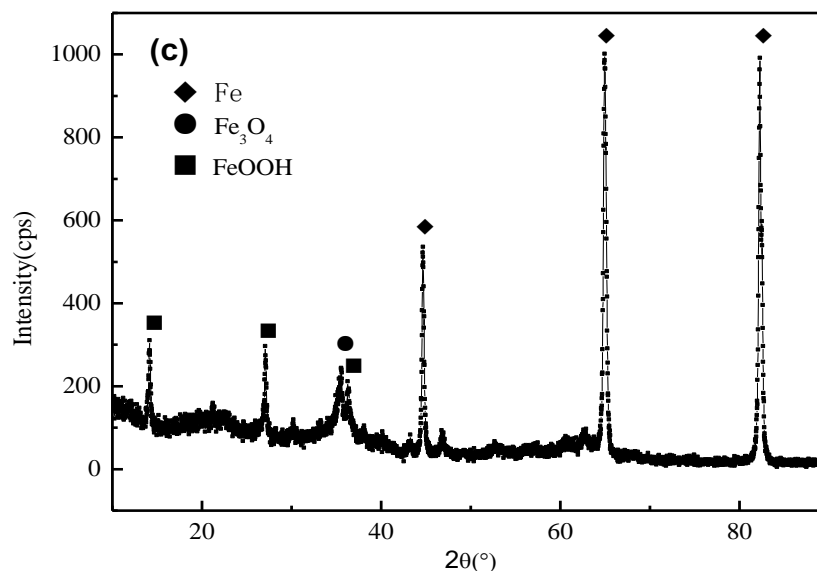
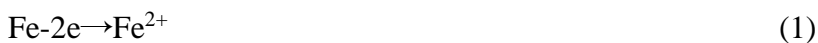


Figure 8. X-ray diffraction results for the corrosion products of the X80 welded joint after immersion in the 3.5% NaCl solution: (a) BM; (b) WZ; and (c) HAZ

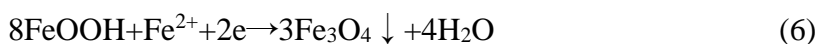
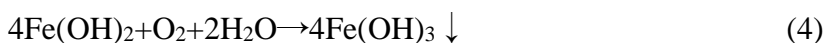
Anode reaction:



Cathode reaction:



Other reactions:



Therefore, the corrosion products of the X80 steel that were formed in the 3.5% NaCl solution were mainly Fe₃O₄ and FeOOH, as shown by the white products in Fig. 3.

3.3 Discussion

The differences among the three zones (BM, WZ and HAZ) is related to the corrosion resistances of their microstructures. The BM microstructure is primarily composed of GB, the WZ microstructure is mainly composed of AF, and the HAZ microstructure is a mixed structure that consists of GB and a small amount of BF.

For the BM, the GB is a mixture of ferrite that is surrounded by islands, and the microstructure is relatively uniform compared to the microstructures of the other zones. These characteristics can reduce the potential difference of the anode and cathode during the corrosion process, and thus the

corrosion rate is reduced in the BM. Moreover, the interface between the bainite laths is a low angle grain boundary, and this interface has a low interfacial energy and a low concentration of impurities[22]. Therefore, the BM of the X80 welded joint has good corrosion resistance.

The structure of WZ is mainly acicular ferrite, which is composed of a non-metallic inclusion core, ferrite around the inclusion and a peripheral carbon-rich layer. The carbon-rich layer can be regarded as the grain boundary of the acicular ferrite. Because of the uneven chemical composition and low electrode potential in the grain boundary, the corrosion begins at the grain boundary first[23]. In the corrosion process, the carbon-rich layer of acicular ferrite is difficult to corrode, and thus most of the grain boundaries are retained. The acicular ferrite forms a large cathode area in some places (such as within a single austenite grain), which reduces the corrosion rate. Therefore, the weld zone has good corrosion resistance[24]. However, as a result of the intense plastic deformation, there are many inclusions and dislocation defects in the lattice during the transformation of AF[25]. The lattice distortion energies and activities of the weld boundaries are higher than those in the BM because of these defects. Therefore, the WZ is more prone to become corroded than the BM. These results are consistent with those in the literature [26].

From the standpoint of antiseptic properties, the smaller the grain size of the material is, the larger the contact area of the micro-battery, and thus the corrosion rate is higher. The microstructure of the HAZ is primarily coarse GB. The coarse grains and non-equilibrium GB are the main factors that cause the poor corrosion resistance in the HAZ.

4. CONCLUSIONS

The microstructures and corrosion resistances of hot-wire TIG-welded joints composed of X80 pipeline steel were studied via metallographic observations, weight-loss methods, electrochemical experiments and SEM. The main conclusions are as follows:

(1) X80 pipeline steel joints were fabricated with ER70S-G wire via hot-wire TIG welding. The microstructure of the WZ is mainly composed of AF, which has low angle grain boundaries, and it is interlaced in a similar fashion as a woven basket. The transformation of AF can create many inclusions and dislocation defects in the lattice, and thus the corrosion resistance of the WZ reduces in response to the transformation. The coarse grain region of HAZ is a mixture of BF and GB. Additionally, there are small amounts of coarse M-A components. The HAZ has hydrogen absorption properties, and stress concentrations in the HAZ easily become a crack source, which can lead to corrosion.

(2) With the weight-loss method and electrochemical testing, the corrosion resistance of the BM is the best after immersion in the 3.5% NaCl solution, whereas the corrosion resistance of HAZ is the worst; the corrosion resistance results of the WZ in the 3.5% NaCl solution are between those of the HAZ and BM.

(3) After the welded joints were soaked in the 3.5% NaCl solution for 20 days, the corrosion products of the three regions were mainly FeOOH and Fe₃O₄. However, the Fe₃O₄ contents of the WZ and HAZ are lower than that of BM.

(4) The corrosion products, which are granular, compact and thicker after treatment in the 3.5% NaCl solution, have better protective effects for the BM. The corrosion products of the WZ are

unevenly distributed as laminae on the substrate. The corrosion products exhibited a loose wadding shape in the HAZ, which results in poor protection. After the corrosion products were removed, cracks and pits were found on the surfaces of the WZ and HAZ. Therefore, the corrosion resistances of the WZ and HAZ are worse than that of BM.

ACKNOWLEDGMENTS

This work was supported by the National Natural Science Foundation of China (NO.51674056), the Scientific and Technological Research Program of Chongqing Municipal Education Commission (KJ1713344, KJ1601328), the Opening Project of Materials Corrosion and Protection Key Laboratory of Sichuan Province (2016CL15), and the Chongqing Research Program of Basic Research and Frontier Technology (CK2016Z08).

References

1. D. J. Kong, C. D. Ye, *Int. J. Miner. Metall. Mater.*, 21(2014)898.
2. C. F. Dong, K. Xiao, Z. Y. Liu, W. J. Yang and X. G. Li, *Int. J. Miner. Metall. Mater.*, 17(2010) 579.
3. W. Zhou, W. Lan, X. L. Cao, H. D. Deng, Y. B. Yan, X. L. Hou, *Int. J. Electrochem. Sci.*, 13(2018)1283.
4. B. He, C. H. Lu, P. J. Han and X. H. Bai, *Eng. Fail. Anal.*, 59 (2016) 410.
5. P. Liang, X. Li, C. Du and X. Chen, *Mater. Design*, 30 (2009) 1712.
6. J. G. Gonzalez-Rodriguez., M. Casales, V. M. Salinas-Bravo, J. L. Albarran, L. Martinez, *Corrosion*, 58(2002) 584.
7. G. Wei, Y. Fan, *China Petroleum Machinery*, 37(2009)1.
8. P. Liang, C. W. Du, X. G. Li, X. Chen, L. Zhang, *Int. J. Miner. Metall. Mater.*, 16(2009)407.
9. C. F. Dong, K. Xiao, Z. Y. Liu, W. J. Yang, X.G. Li, *Int. J. Miner. Metall. Mater.*, 17(2010)579.
10. M. Wu, X. Chen, C. He, J. Xiao, *Acta Metall. Sinica*, 24(2011) 65.
11. X. Chen, M. Wu, C. He, J. Xiao, *Acta Metall. Sinica*, 46(2010) 951.
12. Z. Y. Liu, C. P. Wang, C. W. Du, X. G. Li, *Acta Metall. Sinica*, 47(2011)1434.
13. B. Y. Wang, L. X. Huo, D. P. Wang, C.Y. Deng, *J. Tianjin University.*, 40(2007)757.
14. C. M. Xu, K. Shi, Y. Zhou, R. F. Zhang, X. Li, Y. L. Lu, T. Z. Yao. *Mater. Mecha. Eng.*,33(2009) 34.
15. J. H. LI, Y. Y. Chen, M. Z. Liu, M. Zhang, *Hot Working Technol.*, 44(2015)66.
16. F. Xie, M. Wu, X. Chen, D. Wang, Z. L. Hu, Y. F. Liu, *J. Central South University(Sci. Technol.)*, 44(2013)424 .
17. C. W. Du, X. G. Li, P. Liang, *J. Mater. Eng. Perform.*, 18(2009) 216.
18. P. Liang, X. G. Li, C W Du, X. Chen, L. Zhang, *Corros. Sci. Protec. Technol.*, 21(2009)20.
19. C. C. Xu, Z. S. Wang, J. L. Wang, *J. Chem. Indus. Eng.*, 56(2005)2373.
20. F. F. Eliyan, E. Mahdi and A. Alfantazi, *Corros. Sci.*, 58 (2012) 181.
21. W. Zhao, H. Zhang, Y. Zou, *Int. J. Electrochem. Sci.*, 12 (2017) 679.
22. S. T. Wang, S. W. Yang, K. W. Gao, X .A. Shen, *Acta Metall. Sinica*, 4(2008)1116.
23. M.G. Fontana, N.D. Greene, *Corros. Eng., Chemical industry press, 1982.*
24. A. G. Huang, Z. Y. Li, S. P. Yu, *Trans China Weld Inst.*, 26(2005)30.
25. A. G. Huang, Y. S. Wang, Z. Y. Li, *J. Mater. Protection*, 37 (2004) 6 .
26. X. L. Zhou, H.R. Li X.Z.Hua, Z.G. Ye, *Trans China Weld Inst.*,32(2011)37.